PERGAMON

Mechanism and Machine Theory 37 (2002) 461–476

MECHANISM AND MACHINE THEORY

www.elsevier.com/locate/mechmt

The modeling of cross-axis flexural pivots

Brian D. Jensen [a,1], Larry L. Howell [b,*]

[a] *Department of Mechanical Engineering, University of Michigan, Ann Arbor, MI 48105, USA*
[b] *Mechanical Engineering Department, Brigham Young University, P.O. Box 24102, Provo, UT 84602-4102, USA*

Received 16 March 1999; received in revised form 6 June 2001; accepted 4 December 2001

Abstract

Cross-axis flexural pivots, formed by crossing two flexible beams at their midpoints, have been used in compliant mechanisms for many years. However, their load–deflection behavior has yet to be appropriately modeled to allow easy analysis and synthesis of mechanisms containing them. This paper uses results of non-linear finite element analysis to investigate this behavior. Based on the analysis, two models for the pivots are presented – one simple and one more complex. The accuracy of the models is demonstrated by comparing results to those measured for pivots made from polypropylene and steel.

1. Introduction

In recent years, much attention has focused on the subject of compliant mechanisms. These mechanisms, which rely on the deflections of some or all of their parts to achieve motion, offer many advantages, such as ease of manufacturing, reduction in part count, and diminished friction and wear. However, the complexity of their motion often makes compliant mechanisms difficult to design. For this reason, a model has been presented which allows the designer to model many compliant elements as rigid-body mechanisms with similar force and deflection characteristics. This "pseudo-rigid-body model" allows a designer to quickly develop the basic configuration of a compliant mechanism [1–3]. The design can then be improved, if necessary, by using non-linear finite element analysis to achieve greater accuracy.

In rigid-body kinematics, mechanisms achieve motion through kinematic pairs, such as pin joints. Because of their usefulness, it is often desirable to use compliant "pin joints" in the design

* Corresponding author. Tel.: +1-801-378-8037; fax: +1-801-378-5037.
E-mail address: lhowell@et.byu.edu (L.L. Howell).
[1] Formerly affiliated with Brigham Young University.

0094-114X/02/$ - see front matter
PII: S0094-114X(02)00007-1

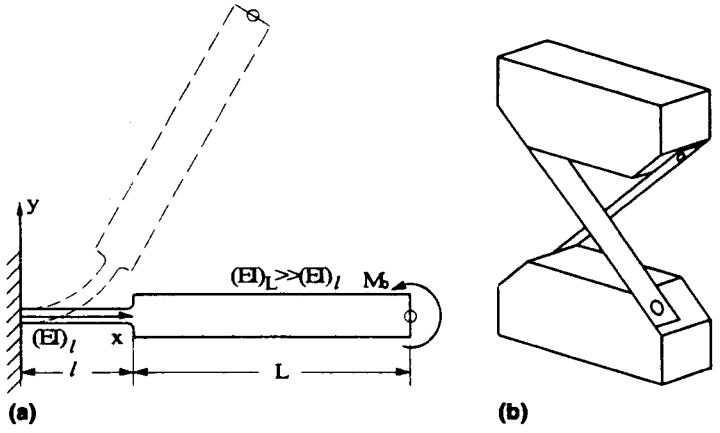

Fig. 1. A small-length flexural pivot (a) and a cross-axis flexural pivot (b). A deflected position of the small-length flexural pivot is shown for clarity. Both pivots may be modeled as compliant "pin joints."

of compliant mechanisms. That is, it is desirable to use compliant segments whose motion is similar to that of a pin joint. One such segment, whose model has already been developed, is the small-length flexural pivot, as shown in Fig. 1(a). This short, thin segment is discussed in further detail in this paper to illustrate its use as a compliant "pin joint." Another compliant element which performs this function is the cross-axis flexural pivot [4,5]. A cross-axis flexural pivot is shown in Fig. 1(b). While this type of pivot has been used for many years, its complex force and deflection characteristics have yet to be represented by a simple, usable model. This paper outlines a simple model for cross-axis flexural pivot deflection. It also presents a second, more accurate model for cross-axis flexural pivot motion. While this second model introduces slightly more complexity, it also decreases modeling error. In order to better compare the characteristics of the small-length flexural pivot and the cross-axis flexural pivot, a review of the model for the small-length flexural pivot will first be presented.

2. Small-length flexural pivots

One way to achieve rotational motion in compliant mechanisms is with a small-length flexural pivot, as shown in Fig. 2(a). Because its rigidity and length are small compared to those of the longer beam, this short segment allows the longer beam to rotate. For a small-length flexural pivot in pure bending, the Bernoulli–Euler equation may be solved to give [1]:

$$\theta_0 = \frac{M_0 l}{EI}, \tag{1}$$

$$\frac{\delta_x}{l} = 1 - \frac{\sin\theta_0}{\theta_0}, \tag{2}$$

$$\frac{\delta_y}{l} = \frac{1-\cos\theta_0}{\theta_0}. \tag{3}$$

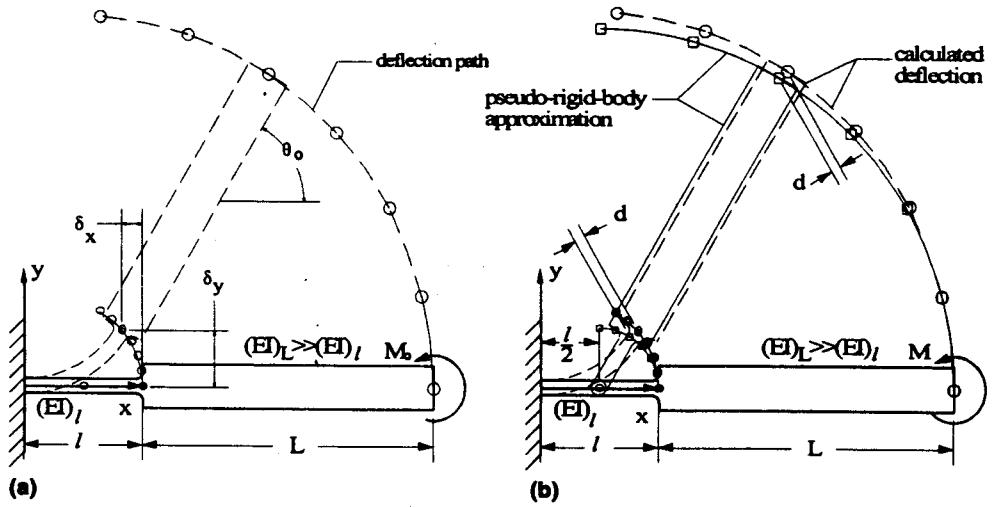

Fig. 2. A small-length flexural pivot shows: (a) motion of a pivot due to an applied moment, and (b) the pseudo-rigid-body model for the pivot. (b) also the error d introduced by the model.

Based on these equations, a pseudo-rigid-body model has been developed [1]. In this model, the small-length flexural pivot is replaced by a pin joint in the center of the pivot, as shown in Fig. 2(b). Then, with $\Theta = \theta_0$,

$$\frac{a}{l} = \frac{1}{2} + \left(\frac{L}{l} + \frac{1}{2}\right)\cos\theta_0, \tag{4}$$

$$\frac{b}{l} = \left(\frac{L}{l} + \frac{1}{2}\right)\sin\theta_0, \tag{5}$$

where a and b are the x- and y-coordinates of the endpoint of the long, rigid segment. The segments resistance to bending is modeled by a torsional spring with stiffness

$$K = \frac{(EI)_l}{l}. \tag{6}$$

Because $\Theta = \theta_0$, the total error introduced by the model is the same at the end of the long beam as at the end of the small-length flexural pivot. Therefore, the absolute error may be found by taking $L = 0$ in Eqs. (4) and (5), and comparing the x- and y- coordinates predicted by Eqs. (2) and (3) with those from (4) and (5). The results are

$$\frac{\varepsilon_x}{l} = \left|\frac{\delta_x}{l} - \left(1 - \frac{a}{l}\right)\right| = \left|\frac{\sin\theta_0}{\theta_0} - \frac{1}{2}(1 + \cos\theta_0)\right|, \tag{7}$$

$$\frac{\varepsilon_y}{l} = \left|\frac{\delta_y}{l} - \frac{b}{l}\right| = \left|\frac{1 - \cos\theta_0}{\theta_0} - \frac{1}{2}\sin\theta_0\right|, \tag{8}$$

$$\frac{d}{l} = \sqrt{\left(\frac{\varepsilon_x}{l}\right)^2 + \left(\frac{\varepsilon_y}{l}\right)^2}. \tag{9}$$

In these equations, ε_x and ε_y are the errors in the x- and y- directions, and d is the total error. Eq. (9) is shown graphically as a function of θ_0 in Fig. 3. This figure shows that a small-length flexural pivot approximates rotational motion with an error of about $0.10l$ for deflections up to 63°, or about 1.1 rad. Note further that, because Eqs. (1) and (2) are based on the assumption of pure bending, Eq. (9) loses some accuracy for the case of applied forces. However, if L is very large compared to l, a vertical force P applied at the end of the long beam may be approximated as a moment of magnitude $P(L + l/2)$. For this case, the equivalent moment becomes much larger than any transverse shear or axial loads, allowing all other loads to be neglected.

3. Pivot stress

Stress developed during pivot motion is another important consideration with small-length flexural pivots. The stress (σ) in a beam due to bending is given by

$$\sigma_{\max} = \frac{Mc}{I}, \tag{10}$$

where M is the moment, c the distance from the central axis, and I is the moment of inertia for the beam cross-section. After solving for M, substituting into Eq. (1), and rearranging, the result is

$$\sigma_{\max} = \frac{\theta_0 cE}{l}. \tag{11}$$

Some error is introduced if the pivot is loaded with a force instead of a moment; however, as explained previously, if $l \ll L$, this error is small. The maximum deflection possible may be found by replacing σ with yield strength (S_y), or, for a brittle material, ultimate strength (S_u) for static failure, or the fatigue strength (S_f) for fatigue failure:

$$\theta_{\max} = \frac{S_{(y,u,f)}l}{cE}. \tag{12}$$

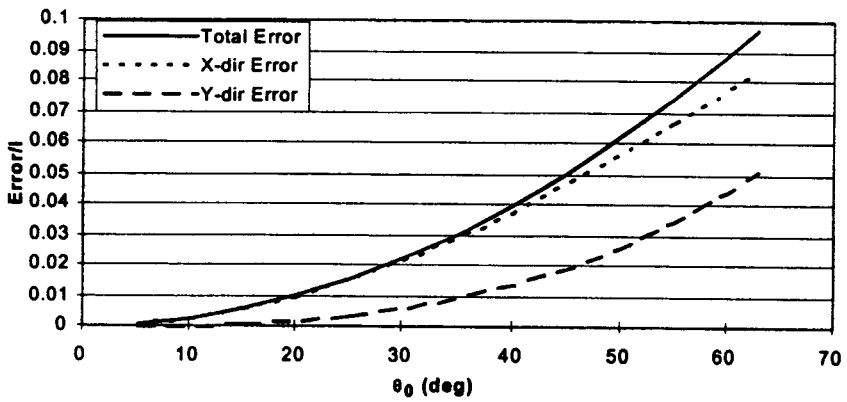

Fig. 3. A graph of the error introduced by the pseudo-rigid-body model. Error is shown as a fraction of l, the length of the small-length flexural pivot.

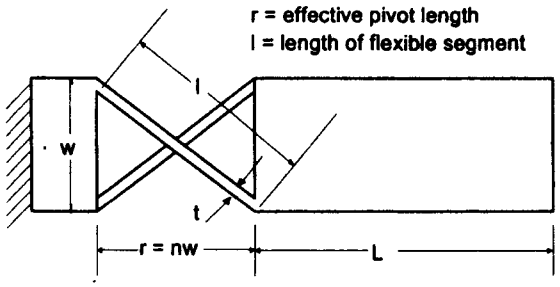

Fig. 4. Diagram of a cross-axis flexural pivot showing dimensional variables.

4. Cross-axis flexural pivots

Fig. 4 outlines the dimensional variables used in this paper to describe the geometry of a cross-axis flexural pivot. Note that r is defined as the effective pivot length, while l denotes the length of a single flexible segment within the pivot. In modeling cross-axis flexural pivots, the non-dimensional parameter n, defined as the effective pivot length divided by the pivot width, is used

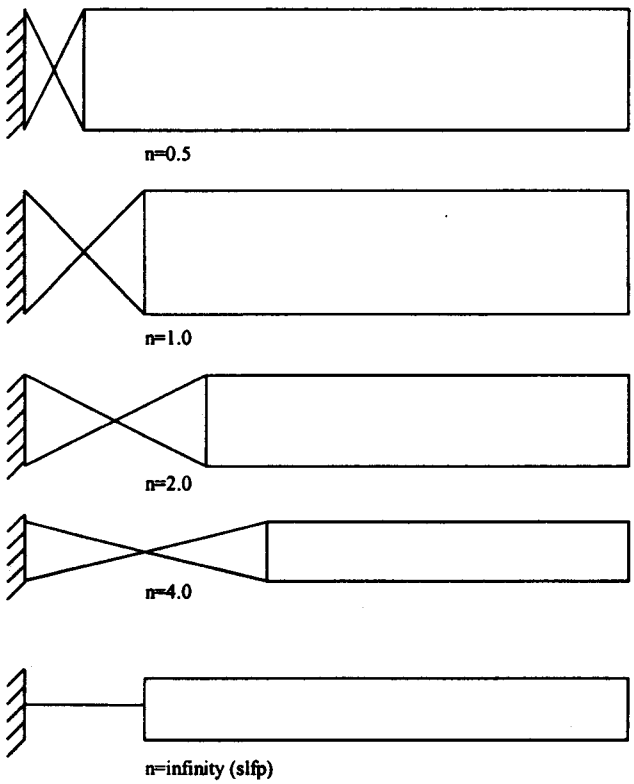

Fig. 5. Various configurations of cross-axis flexural pivots based on varying values of n. Note that as n approaches infinity, the cross-axis flexural pivot becomes a small-length flexural pivot.

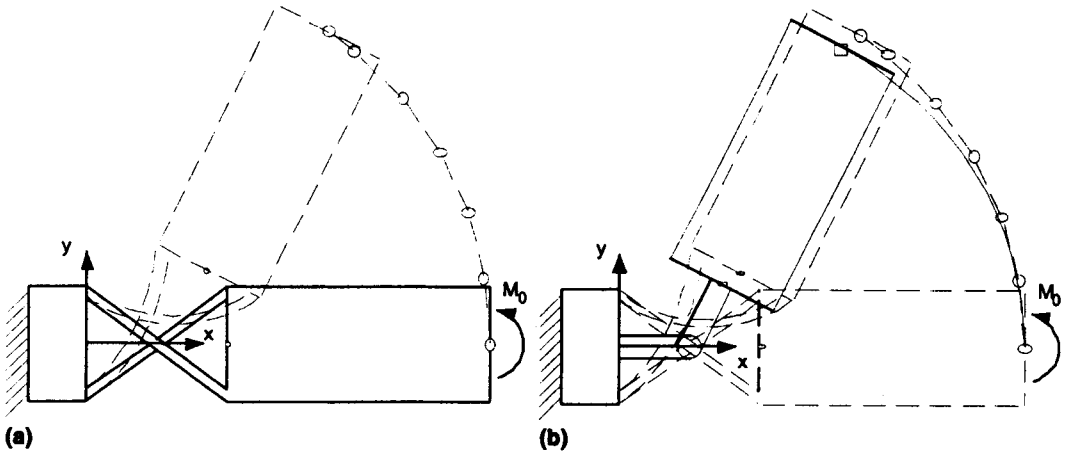

Fig. 6. A cross-axis flexural pivot: (a) shows the deflection path of the pivot, and (b) compares this path to the path described by the model.

to describe the relative geometry of the pivot. Fig. 5 illustrates how changing n changes pivot geometry. With n and w specified, the length of the flexible section, l, may then be expressed as

$$l = w\sqrt{1+n^2} \tag{13}$$

so that the ratio of flexible length to effective pivot length is

$$\frac{l}{r} = \frac{\sqrt{1+n^2}}{n}. \tag{14}$$

Analysis of Eq. (14) shows that, as n becomes large, the ratio of flexible length (l) to effective length (r) rapidly decreases to one, so that the cross-axis flexural pivot behaves like a small-length flexural pivot, as shown in Fig. 5. Conversely, the ratio of flexible length to effective length is greatest when n is small.

Because the motion of cross-axis flexural pivots is more complex than that of small-length flexural pivots, closed-form equations for deflection are not available. However, finite element analysis gives very accurate solutions for deflection, and these solutions have been analyzed to develop a simplified model for cross-axis flexural pivots. This is done by comparing the FEA solutions to various models, and then optimizing model constants by minimizing the error introduced by the models over a 1.1 rad deflection. This deflection is considered to be appropriately large to allow modeling of any deflection expected in actual usage. A commercial FEA program capable of nonlinear analysis (ANSYS) is used, with elastic beam elements, to obtain the results.

5. The pin-joint model

A cross-axis flexural pivot may be modeled most simply using a pin joint located at the center of the pivot, as shown in Fig. 6. Fig. 7 shows the error associated with this model, based on finite element results, as a function of n for a deflection of 1.1 rad (about 63°). Note that the error represents the degree of translation present in the primarily rotational motion at the pivot. As

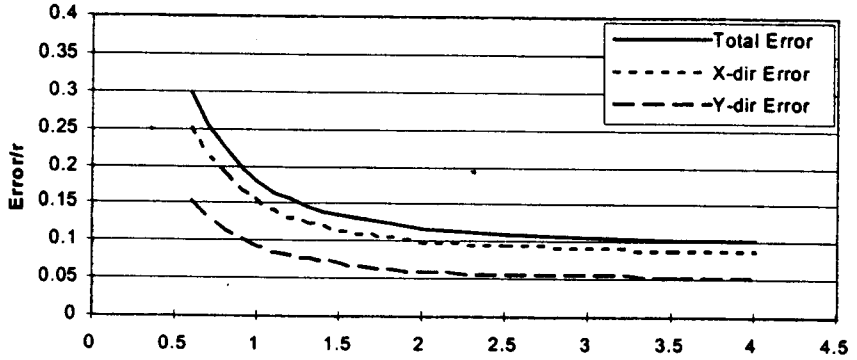

Fig. 7. Normalized model error for a 1.1 rad deflection of a cross-axis flexural pivot. As n becomes large, the error is about 10% of r, which is the model error of a small-length flexural pivot at 1.1 rad, as shown in Fig. 3.

expected, the error begins to converge for large n to that for a small-length flexural pivot (about 10%, as shown in Fig. 3). Although Fig. 7 indicates fairly large error for small values of n, it should be remembered that the error represented is for a 1.1 rad deflection. Smaller deflections introduce much less error.

Finite element modeling revealed a nearly linear relationship between the applied moment and the angular deflection of the pivot. Therefore, the resistance of the pivot to bending is modeled by a torsional spring. Following the development of [3], the spring stiffness may be given by

$$K = \frac{K_\Theta EI}{2l}, \tag{15}$$

where E is Young's modulus, I is the moment of inertia of the flexible sections, l is the length of the flexible segments, and K_Θ is known as the "stiffness coefficient". This stiffness coefficient is determined by finding the value which minimizes the error in pivot stiffness over a deflection of 1.1 rad. The optimization problem may be stated as: *Find the value of the stiffness coefficient, K_Θ, which minimizes the sum of the error in predicted moment over a 1.1 rad deflection.* The sum of error was approximated by summing error over 22 discrete points across the 1.1 rad deflection.

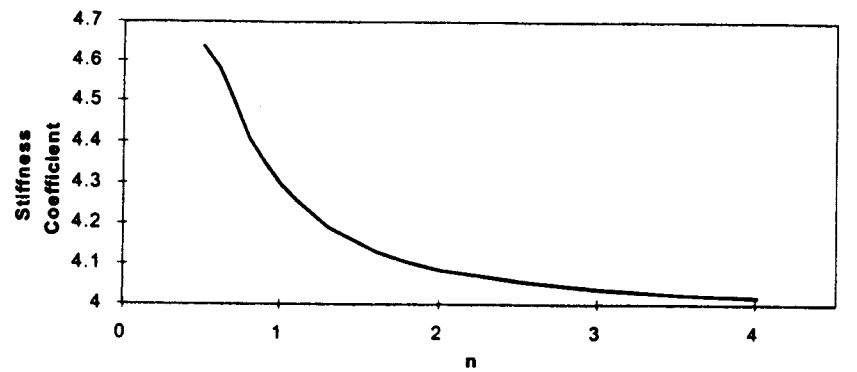

Fig. 8. A graph of the stiffness coefficient based on n. The stiffness coefficient is determined by optimizing K_Θ to minimize error over the 1.1 rad deflection.

Fig. 8 shows K_Θ as a function of n after solving the optimization problem above. Applying a polynomial curve-fit to the graph yields the function

$$K_\Theta = 5.300185 - 1.6866n + 0.885356n^2 - 0.2094n^3 + 0.018385n^4. \quad (16)$$

For this curve, the correlation coefficient equals 0.99910. In addition, $0.5 \leqslant n \leqslant 4.0$.

6. The four-bar model for cross-axis flexural pivots

The model outlined in the preceding paragraphs is adequate for design purposes; in particular, its simplicity makes it a valuable tool. However, it is possible to create a model which more accurately predicts the motion and force characteristics of a cross-axis flexural pivot. The pivot shown in Fig. 6 is symmetrical about a line through its center (the line of symmetry is vertical when undeflected and otherwise is the bisector of the deflection angle). This symmetry allows the cross-axis flexural pivot to be modeled as a four-bar mechanism, as shown in Fig. 9(a). In this model, pin joints are located at the ends of the flexible segments at the edge opposite the direction of motion. Two more pin joints are located a distance of γl along the flexible segments, where γ is the "characteristic radius factor," as defined in [2]. This factor allows the pin joints to be placed at any arbitrary distance along the flexible segments, so that the model can be optimized to give the best deflection characteristics. Note also that this placement of the pin-joints models pivot motion in only one direction; however, motion in the opposite direction is symmetrical. Torsional springs of identical spring stiffness K are placed at each pin joint to model the stiffness of the pivot. The motion of this four-bar mechanism may then be determined using standard rigid-body kinematics. The following section shows how this may be done.

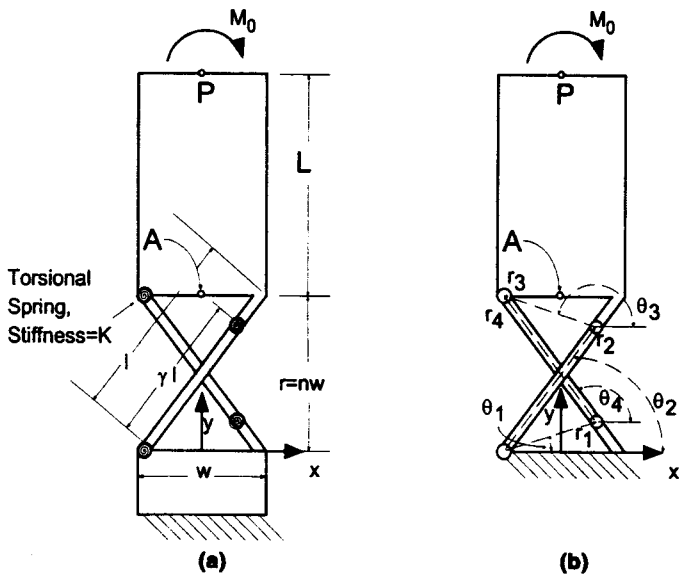

Fig. 9. The four-bar model of a cross-axis flexural pivot. Note that this model only applies for motion in one direction.

Generally, the angle of the long, rigid beam (θ_3, as shown in Fig. 9(b)) is known, and the angles of the links 2 (θ_2) and 4 (θ_4) must be determined. This may be done by solving the Freudenstein equations [6]:

$$r_2 \cos\theta_2 + r_3 \cos\theta_3 = r_1 \cos\theta_1 + r_4 \cos\theta_4, \tag{17}$$

$$r_2 \sin\theta_2 + r_3 \sin\theta_3 = r_1 \sin\theta_1 + r_4 \sin\theta_4. \tag{18}$$

Note also that

$$r_2 = r_4 = \gamma l \tag{19}$$

and

$$r_1 = r_3 = \sqrt{(\gamma w)^2 + r^2(1-\gamma)^2}, \tag{20}$$

where γ is yet to be determined by minimizing model error.

With equations developed for the motion of the four-bar mechanism, the value of γ can be found which minimizes deflection error over a 1.1 rad angular deflection. The same technique was used as outlined earlier for K_Θ. Fig. 10 shows a graph of the best value of γ based on n. The best-fit polynomial for γ is

$$\gamma = 2.208105 - 10.0489n + 27.83212n^2 - 37.7021n^3 + 25.032n^4 - 6.5358n^5,$$
$$0.5 \leqslant n < 1.0, \tag{21}$$
$$\text{correlation coefficient} = 0.9999,$$

$$\gamma = 0.811175 - 0.03329n + 0.008143n^2 - 0.00075n^3,$$
$$1.0 \leqslant n \leqslant 4.0, \tag{22}$$
$$\text{correlation coefficient} = 0.9999.$$

Finite element analysis of the error resulting from use of this model shows that total error is generally well below 1% of the effective pivot length r.

As shown in Fig. 9(a), the resistance of the pivot to bending is modeled by torsional springs, with stiffness K, placed at each of the four joints. The spring stiffness may be given as

$$K = \gamma K_{\Theta.\mathrm{fb}} \frac{EI}{l}, \tag{23}$$

where $K_{\Theta.\mathrm{fb}}$ is the stiffness coefficient. The subscript fb is used to differentiate between the four-bar model stiffness coefficient and that of the pin-joint model. $K_{\Theta.\mathrm{fb}}$ is determined by minimizing error

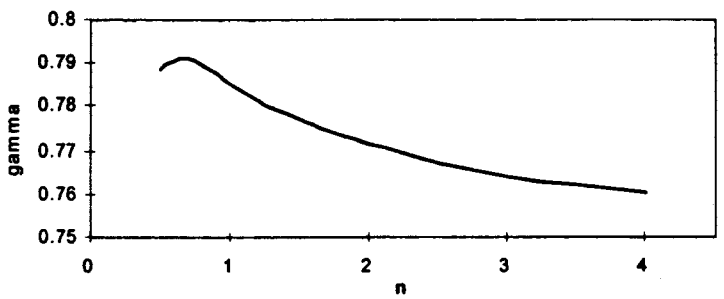

Fig. 10. Variation of γ with n. γ is determined by minimizing error for motion up to 1.1 rad.

in the applied moment required for deflections up to 1.1 rad, as previously explained. Fig. 11 shows $K_{\theta,fb}$ as a function of n. $K_{\theta,fb}$ may also be given as a polynomial curve-fit as

$$K_{\theta,fb} = 1.075835 + 6.818114n - 13.6023n^2 + 11.52314n^3 - 3.53289n^4,$$
$$0.5 \leqslant n < 1.0, \tag{24}$$
$$\text{correlation coefficient} = 0.99969,$$

$$K_{\theta,fb} = 2.241032 + 0.047655n - 0.00491n^2,$$
$$1.0 \leqslant n \leqslant 4.0, \tag{25}$$
$$\text{correlation coefficient} = 0.99965.$$

Once the spring stiffness is determined, the overall moment–deflection characteristics of the pivot may be found using the principle of virtual work [7] as

$$M_0 = T_2 + T_3 - (T_1 + T_2)\frac{r_3 \sin(\theta_3 - \theta_4)}{r_2 \sin(\theta_4 - \theta_2)} - (T_3 + T_4)\frac{r_3 \sin(\theta_3 - \theta_2)}{r_4 \sin(\theta_4 - \theta_2)}, \tag{26}$$

where

$$\begin{aligned} T_1 &= K(\theta_2 - \theta_{20}), \\ T_2 &= K(\theta_2 - \theta_{20} - \theta_3 + \theta_{30}), \\ T_3 &= K(\theta_4 - \theta_{40} - \theta_3 + \theta_{30}), \\ T_4 &= K(\theta_4 - \theta_{40}) \end{aligned} \tag{27}$$

and the "0" subscripts represent undeflected values of the angles.

7. Pivot stress

The maximum deflection which a cross-axis flexural pivot can achieve is determined by the stress in the flexural arms. Therefore, it is desirable to have an expression relating maximum stress in the pivot to angular motion. If a conservative, easy estimate is required, the stress in the pivot can be approximated as the stress in a small-length flexural pivot of the same pivot length. A

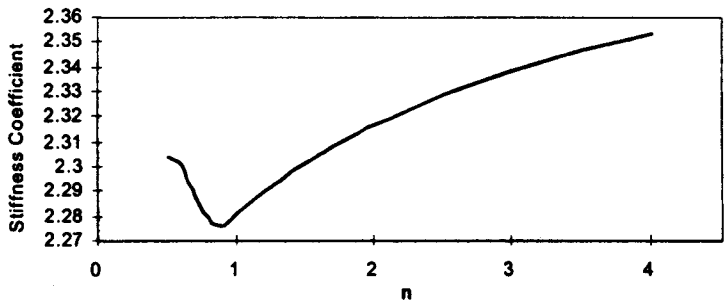

Fig. 11. $K_{\theta,fb}$ based on n. The stiffness coefficient is found by minimizing error over a 1.1 rad deflection.

slightly more accurate expression models the stress linearly with respect to θ. Then, the maximum stress in the pivot may be approximated by

$$\sigma = \frac{S_\Theta \theta E t}{2r}, \tag{28}$$

where t is the thickness of the flexible segment, E is the modulus of elasticity, r is the pivot length as defined in Fig. 6, and S_Θ is the "stress coefficient," a parameter that corrects the stress estimate based on n. Fig. 12 shows a graph of S_Θ based on n. S_Θ may also be given as a curve-fit as

$$S_\Theta = 0.062998 + 1.884218n - 1.43653n^2 + 0.551786n^3 - 0.10523n^4 + 0.007889n^5,$$
$$0.5 \leqslant n \leqslant 4.0, \tag{29}$$
$$\text{correlation coefficient} = 0.99988.$$

Comparing Eq. (28) with Eq. (11) shows that S_Θ is a factor relating the maximum stress in a cross-axis flexural pivot with the stress expected in a small-length flexural pivot of the same length, and with the same flexural thickness, as the cross-axis flexural pivot. Therefore, if S_Θ is less than one, the cross-axis flexural pivot is expected to have lower stress than a small-length flexural pivot of the same overall pivot length. Consulting Fig. 12, it can be seen that cross-axis flexural pivots exhibit the best stress characteristics for $n < 1.2$. For higher n, the cross-axis flexural pivot actually has slightly more stress, averaged over the 1.1 rad deflection, than the small-length flexural pivot. This is because additional stresses caused by the complex motion of the cross-axis flexural pivot are higher than the stress reduction caused by the added length of the flexural members. However, the cross-axis flexural pivot stress remains within 7% above the small-length flexural pivot stress, so this small difference can often be ignored.

The relationship in Eq. (28) remains conservative over most deflections; however, it actually *underpredicts* stress for large deflections. This is because the actual relationship between stress and

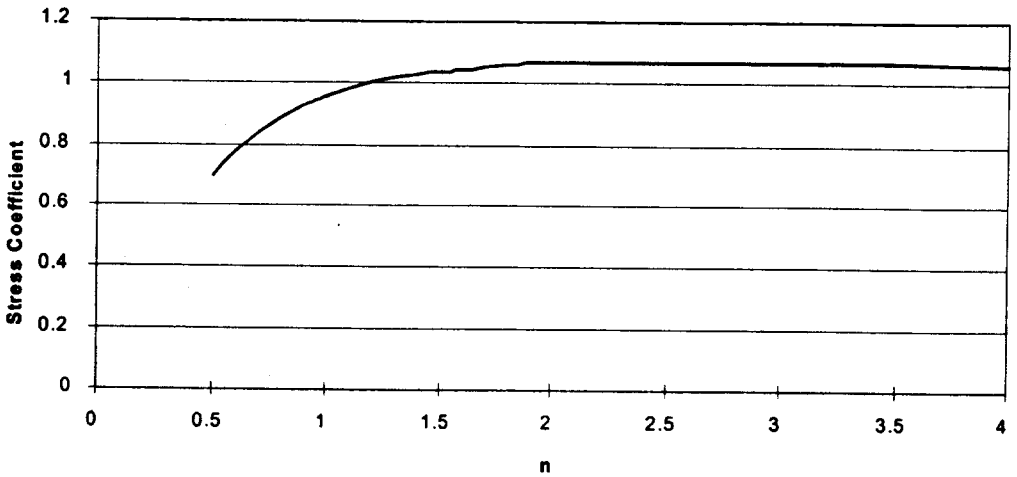

Fig. 12. A graph of S_Θ based on n. S_Θ reflects the fraction of stress in a cross-axis flexural pivot compared to a small-length flexural pivot of the same pivot length and flexural thickness.

deflection angle can be better modeled as quadratic rather than linear. Therefore, an even more accurate relationship is

$$\sigma = \frac{Et}{2r}(S_1\theta + S_2\theta^2), \tag{30}$$

where S_1 and S_2 are coefficients based on n. The correlation between this equation and the stress data predicted by finite element analysis is greater than 0.999 for all values of n. S_1 and S_2 are shown graphically in Fig. 13. They may also be represented as

$$S_1 = 0.189394 + 0.899845n - 0.4333n^2 + 0.097866n^3 - 0.00839n^4,$$
$$\text{correlation coefficient} = 0.9999, \tag{31}$$

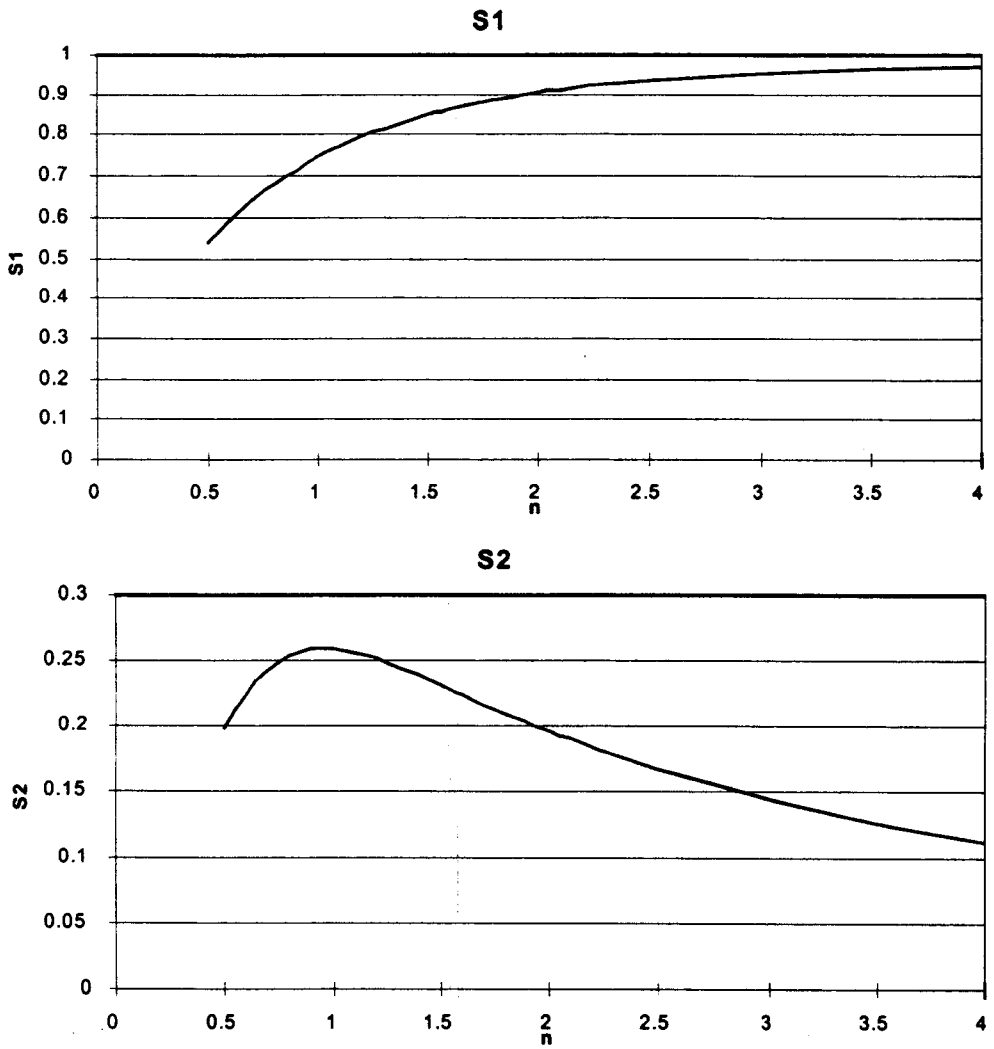

Fig. 13. Graphs of S_1 and S_2 based on varying values of n. S_1 and S_2 are the model coefficients for the parabolic stress model.

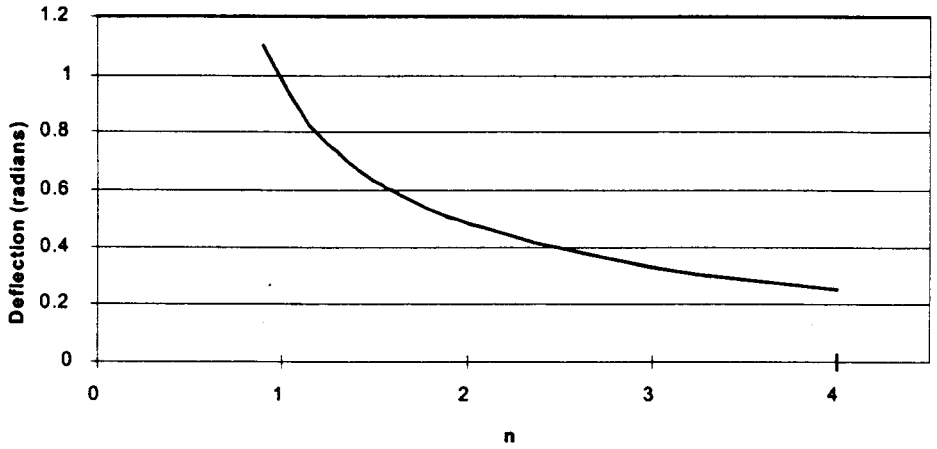

Fig. 14. A graph of angular deflection which results in equal stress for a small-length flexural pivot and a cross-axis flexural pivot. n determines the geometry of the cross-axis flexural pivot.

$$S_2 = -0.09799 + 0.982995n - 0.96184n^2 + 0.413319n^3 - 0.08387n^4 + 0.006530n^5, \quad \text{correlation coefficient} = 0.9994. \tag{32}$$

Because the stress in the cross-axis flexural pivot increases approximately quadratically with angle, it tends to be smaller than small-length flexural pivot stress for small deflections, but it increases until it exceeds small-length flexural pivot stress at some angular deflection. Fig. 14 shows the angle at which the stress equals that of a small-length flexural pivot for varying values of n. To use this graph, the small-length flexural pivot and cross-axis flexural pivot must have equivalent values for effective pivot length and flexural thickness. For n less than 0.9, the cross-axis flexural pivot stress remains below the small-length flexural pivot stress for deflections greater than 1.1 rad. However, as n increases, the angular deflection for equal stress drops rapidly until it is about 0.22 rad (13°) for $n = 4$. Therefore, for situations where pivot stress is an important concern, a cross-axis flexural pivot with $n = 4$ will perform better than a similarly sized small-length flexural pivot for deflections below 13°. This information can prove very valuable in design.

8. Model validation

To validate the model, two cross-axis flexural pivots were fabricated, one each from polypropylene and spring steel. The dimensions of each pivot, as defined in Fig. 6, are given in Table 1. The deflection paths and moment–displacement characteristics were measured for each pivot, and they were compared to the predictions of finite element analysis as well as each of the two models.

Table 1
Dimensions of the two test pivots

	n	w (cm)	r (cm)	I (cm^4)	L (cm)
Polypropylene	0.762	3.3	2.5	2.1×10^{-4}	4.1
Spring steel	0.75	4.0	3.0	5.6×10^{-6}	5.0

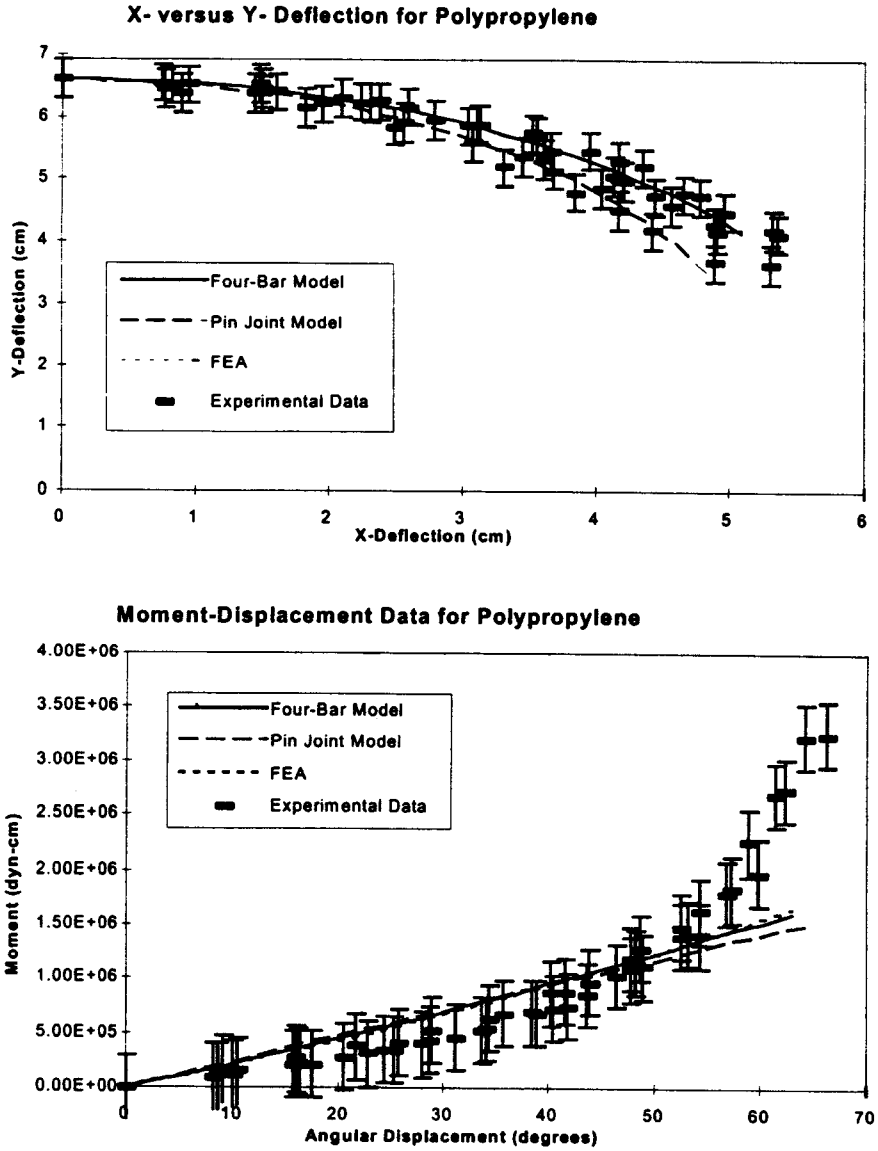

Fig. 15. Graphs showing results of experiments with the polypropylene cross-axis flexural pivot. The data follows the predictions of the models and of finite element analysis fairly well, although some deviation is evident in the moment–deflection curve.

Data were gathered and averaged over six deflections of the polypropylene pivot and eight of the steel pivot. The graphs of data for the polypropylene model are shown in Fig. 15, and the data for the steel pivot are shown in Fig. 16. The finite element data and the four-bar model agree quite well with the experimental data in general. The pin-joint model, while being very good for the moment–deflection data, predicts the x- and y-displacements somewhat less accurately. However, it is accurate enough for many purposes, especially considering its simplicity. The tests performed, therefore, validate the models.

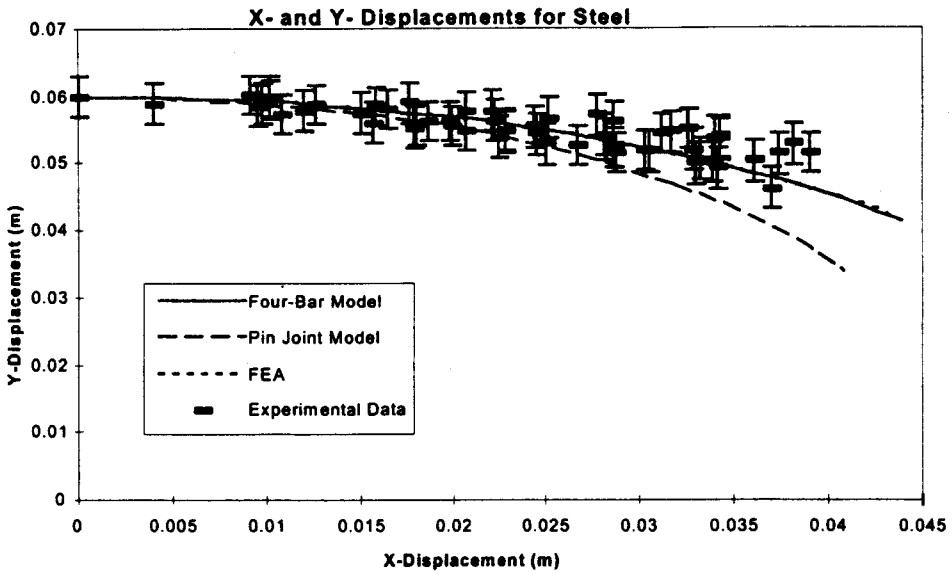

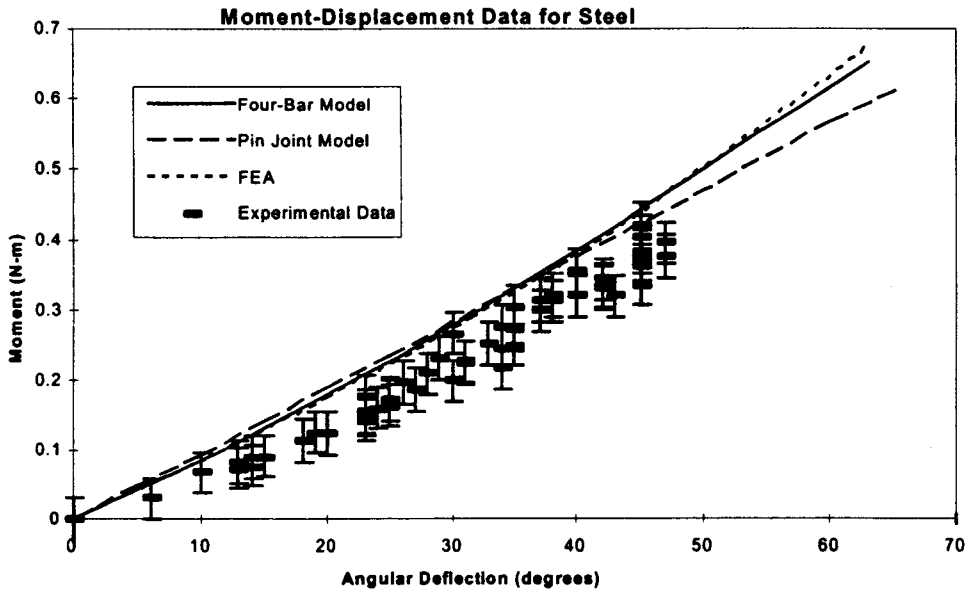

Fig. 16. Experimental data for the steel cross-axis flexural pivot.

9. Conclusion

In this paper, the load–deflection characteristics of cross-axis flexural pivots have been studied using non-linear finite element analysis, allowing a pseudo-rigid-body model to be proposed. The results show that the pivot approximates the motion of a pin joint, with the stiffness of the pivot modeled using a torsional spring placed at the center of the joint. The pivot was compared to a

small-length flexural pivot to demonstrate its usefulness as a compliant "pin joint". If further accuracy is desired, the cross-axis flexural pivot may also be modeled using a four-link mechanism with torsional springs at each joint. Optimal link lengths and values of the torsional spring constants were found by minimizing error in both motion and stiffness over a large deflection. The stress in the pivot during motion was also studied. Based on the analysis, it is recommended that the ratio of pivot length to pivot width be between 0.5 and 1.0 for lowest stress. The deflection models were validated by measuring the load–deflection data for two different small-length flexural pivots made from polypropylene and spring steel. The results agreed in each case with the predictions of the models, with the four-bar model predicting the pivot motion slightly better. The models developed may be used for analysis or synthesis of compliant mechanisms which contain cross-axis flexural pivots.

Acknowledgements

The authors gratefully acknowledge the National Science Foundations support of this work through a graduate fellowship and Career Award, No. DMI-9624574.

References

[1] L.L. Howell, A. Midha, ASME Journal of Mechanical Design 116 (1) (1994) 280–290.
[2] L.L. Howell, A. Midha, ASME Journal of Mechanical Design 117 (1) (1995) 156–165.
[3] L.L. Howell, A. Midha, T.W. Norton, ASME Journal of Mechanical Design 118 (1) (1996) 126–131.
[4] W.D. Weinstein, Machine Design (June 10, 1965) 150–157.
[5] W.D. Weinstein, Machine Design (July 8, 1965) 136–145.
[6] B. Paul, Kinematics and Dynamics of Planar Machinery, Prentice-Hall, Englewood Cliffs, NJ, 1979.
[7] L.L. Howell, Compliant Mechanisms, Wiley, New York, 2001.